MODELING THERMAL EXPANSION OF A LARGE AREA EXTRUSION DEPOSITION ADDITIVELY MANUFACTURED PARTS USING A NON-HOMOGENIZED APPROACH

Dylan Hoskins[1], Seokpum Kim[2], Ahmed Hassen[2],
John Lindahl[2], Vlastimil Kunc[1,2], Chad Duty[1,2]

[1] University of Tennessee, Knoxville
[2] Manufacturing Demonstration Facility, Oak Ridge National Laboratory

Abstract

Interest in the use of large area extrusion deposition additive manufacturing (LAEDAM) to create tools for creation of composites is on the rise, due to its ability to create complex shapes rapidly. To ensure the parts created from the tool meet geometric standards, it is important to understand the thermal expansion of the printed part. Which is a challenge as LAEDAM imparts a non-uniform fiber orientation to the deposited material. A non-uniform fiber orientation in the deposited material creates a non-homogeneous cross section at a given position. Due to this heterogeneity, the coefficient of thermal expansion (CTE) also varies according to the position in the cross section. Previous modelling attempts of LAEDAM parts have employed a homogenized approach. This work experimentally characterizes CTE variations across the cross section of a bead using thermomechanical analysis and uses this as a non-homogenized input at the bead level for a finite element model. Predictions from this finite element model are then be compared to strain maps measured using 2-D digital image correlation of large-scale printed parts (127 mm cubes).

Introduction

Extrusion deposition additive manufacturing (EDAM), commonly referred to as 3D printing, is a field of growing interest in the engineering and scientific community at large. EDAM allows for rapid construction of parts by depositing thermoplastic using specified paths in a layer and building the part layer by layer. The process also allows for complex geometries, such as sparse infills and contoured interiors, that may be difficult or simply not possible with traditional (subtractive) manufacturing techniques. Until recently (within the last decade), the EDAM process was used to produce small parts (less than .1 m^3 volumetrically). However, in 2014 EDAM was utilized to create parts orders of magnitude larger than previously demonstrated, a variation that this work will refer to as large area extrusion deposition additive manufacturing (LAEDAM). LAEDAM opened a new world of possibilities to explore, one of particular interest is the printing autoclave mold for composites used in the aerospace industry. However, with this possibility comes additional challenges that are absent in small scale EDAM and understanding the thermal expansion behavior is critical for autoclave tools.

THIS MANUSCRIPT HAS BEEN AUTHORED BY UT-BATTELLE, LLC UNDER CONTRACT NO. DE-AC05-00OR22725 WITH THE U.S. DEPARTMENT OF ENERGY. THE UNITED STATES GOVERNMENT RETAINS AND THE PUBLISHER, BY ACCEPTING THE ARTICLE FOR PUBLICATION, ACKNOWLEDGES THAT THE UNITED STATES GOVERNMENT RETAINS A NON-EXCLUSIVE, PAID-UP, IRREVOCABLE, WORLDWIDE LICENSE TO PUBLISH OR REPRODUCE THE PUBLISHED FORM OF THIS MANUSCRIPT, OR ALLOW OTHERS TO DO SO, FOR UNITED STATES GOVERNMENT PURPOSES. THE DEPARTMENT OF ENERGY WILL PROVIDE PUBLIC ACCESS TO THESE RESULTS OF FEDERALLY SPONSORED RESEARCH IN ACCORDANCE WITH THE DOE PUBLIC ACCESS PLAN (HTTP://ENERGY.GOV/DOWNLOADS/DOE-PUBLIC-ACCESS-PLAN).

One large challenge in utilizing parts produced via EDAM of any size is the anisotropy that is caused by the process, material location and orientation (print paths) and creation of the part layer by layer. Anisotropy and how various print parameters affect the material properties in each direction have been studied extensively (1-6). A major contributor to the anisotropy is the inherent heterogeneous structure of the part, where the part will exhibit higher tensile strength and elastic modulus in the direction in which the most print paths align. The anisotropy is found in parts produced from both neat and fiber reinforced feedstock, a necessity for LAEDAM to minimize warpage of the part. Parts produced from fiber reinforced feedstock exhibit higher strength and stiffness, but they have higher anisotropy than their neat counterparts (7-12). This anisotropy is due to the shear alignment of fibers during the printing process (13-16). Composite material will demonstrate properties, more similar to the reinforcing fibers in the direction in which most of the fibers are aligned and more similar to the matrix in the direction, or directions, with less fiber alignment. The fiber orientation in LAEDAM beads is complex and varies considerably depending on the location within the bead (17-19). Fiber orientation is directly linked with material properties such as stiffness, tensile strength and CTE, meaning these properties will also vary throughout a LAEDAM bead (20,21). Thus, a part is created of beads with complex fiber orientation profiles, which make up complex print paths in each layer, finally forming the part. This hierarchical structure of complexities makes it hard to predict or even measure thermal expansion, which is necessary to ensure autoclave tools can produce parts for the aerospace industry.

The hierarchical structure and size of the part, on the meter scale, means that traditional methods of measuring CTE such as TMA, where the sample size is around 0.2-0.4 in in any direction, is not directly applicable. Due to the variation of fiber alignment throughout the bead multiple samples are required to fully characterize the CTE variation in a singular bead. However, utilization of digital image correlation (DIC) allowed for measurement of the thermal expansion of an entire LAEDAM part (127mm cube). In this work, two finite element analysis (FEA) models were used to predict the CTE of a printed LAEDAM part. The input for the FEA model was CTE measurements in the x-, y- and z-directions from seven samples taken from seven different locations throughout the width of a bead. The FEA models were then compared to the CTEs measured using DIC.

Experimental Methods and Modelling

A total of three cubes were printed for this study, each cube was printed on the Manufacturing Demonstration Facility's BAAM printer at 10.16mm nozzle at 200° C using 20% carbon fiber by weight acrylonitrile butadiene styrene (ABS) from Techmer PM (ES Electrafil® J-1200/CF/20 NAT ABS). Two of the cubes were printed larger than 127mm in each direction then milled down to 127 mm cubes with parallel sides with each side parallel to a respective print direction. One of the 127mm cubes was printed with unidirectional layers all in the same orientation, which will be referred to as the 0-0 cube. The other 127mm cube, the 0-90 cube, was printed with unidirectional layers, but each layer rotated 90 degrees from the precious layer. The third cube was milled to a 50.8 mm cube to be used for sectioning purposes and printed with 0-0 orientation.

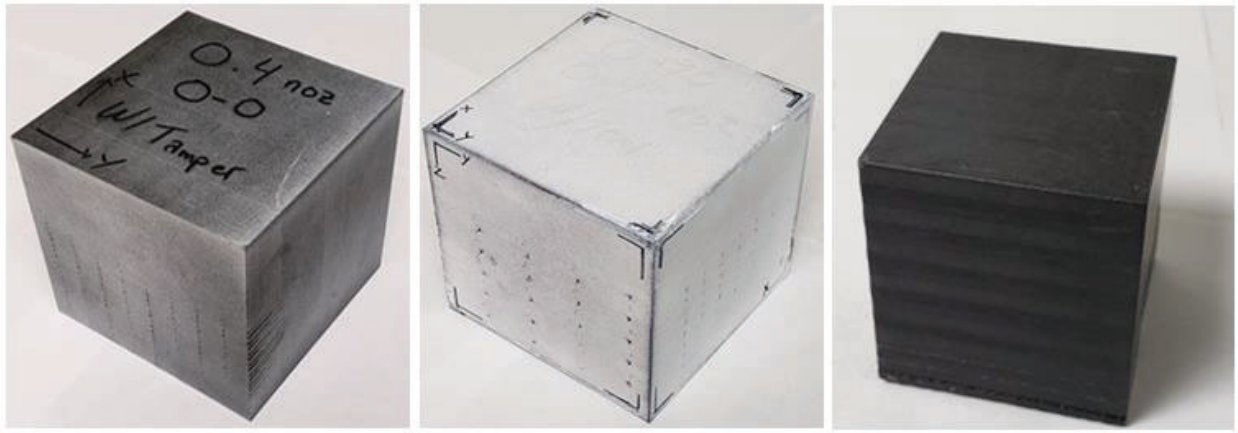

Figure 1 Images of the samples used in this work (a) 127 mm 0-0 cube for DIC, (b) 127 mm 0-90 cube after DIC preparation, (c) 50 mm 0-0 cube for TMA samples

For the DIC measurements, the 5-inch cubes were used as the specimens for measurement. Once the samples were machined, the cubes were painted white and the axes of the cubes were labelled with the x-direction being the direction parallel with the deposition, the y-direction being the direction perpendicular and in-plane with the x-direction and the z-direction is the build direction. It should be noted that the in the 0-90 cube the x- and y-direction are arbitrary due to the perpendicular stacking. The painted cubes were then speckled with black ink using a rubber stamp and the same speckling procedure. Each cube followed the same procedure for measuring CTE, the cube was placed in the furnace with a viewport at room temperature. Forty-five images of the cube were then captured, every 100ms using a National Instruments cDAQ™-9174, of the cube in the furnace. Next, the temperature in the furnace was increased to 90°C at a rate of 150 °C per hour, the cube was then allowed to equilibrate for 12 hours. Forty-five photos were then taken at 90°C, also every 100ms. Strain maps were created for the x- and y-directions, using Vic-Snap 2D software, by comparing each of the photos to a reference photo of the cube taken at room temperature. The strain maps for each photo set were then averaged to create four representative strain maps for each cube, two at room temperature (x and y strain) and two at high temperature (x and y strain). Strain measured at low temperature is considered to be system noise, as no strain has occurred. Data from the four average strain maps are then used to calculate the average strain in the cube in the x- and y- direction. Average strain is then divided by the difference in temperature between room temperature and 90°C to calculate the x- and y- CTE of the cube, can be seen in equation below.

$$CTE_i = \frac{\epsilon_i^{High\ Temp} - \epsilon_i^{Low\ Temp}}{\Delta T}$$

For TMA measurements, the remaining 2-inch cube was used as the sample for cutting TMA samples out of. A diamond saw, Buehler Isomet 1000, was used to cut off a section of the cube that was comprised of three beads in width, two layers tall and two inches in length. Part of the section was then cut into TMA samples, also using a diamond saw, from with the following

dimensions: 7mm in the x-direction and 5 mm in the y- and z-directions. Samples were collected from seven locations throughout the width of the bead which can be seen in Figure 2. Samples were cut carefully to ensure samples with the same location in the width of the bead were aligned in the length of the bead. Each of the samples was then allowed to dry in a vacuum furnace at 75 °C for 12 hours, then stored in a desiccator until the start of the experiment. Thermomechanical analysis was performed on a TA Instruments Q400 TMA. Analysis was carried out, in triplicate, for each of the samples in each direction, between room temperature and 90°C. CTE was calculated, using TA Instruments Universal Analysis, by determining the slope of a line fitted to the dimensional change and temperature data between the two temperatures.

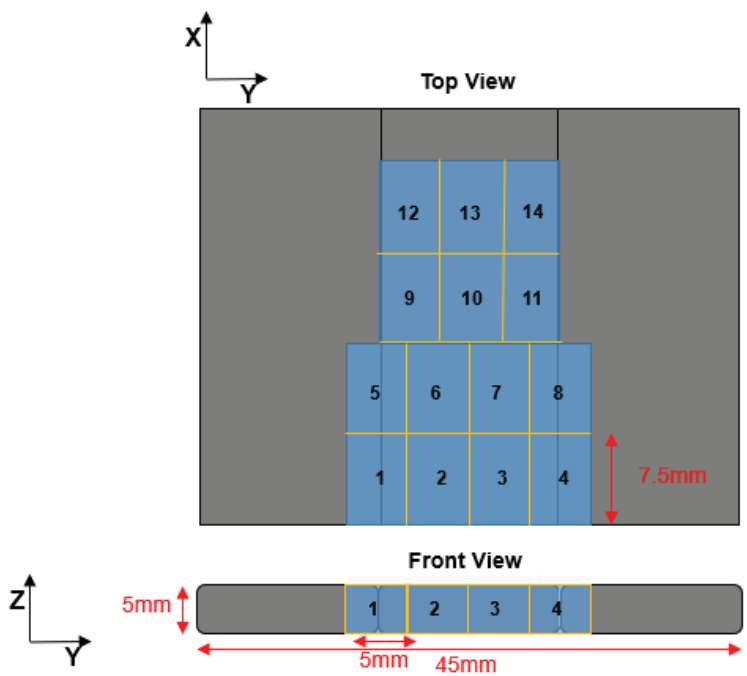

Figure 2 Depiction of TMA sample location within the printed bead

The finite element models used to simulate the thermal expansion of the LAEDAM printed parts in this work were created in a manner mimicking the actual printed structure. Concentric extruded ellipses were used to represent each printed bead, which is represented in Figure 3, as fiber orientation varies depending on location within the bead. The beads in the actual part were measured and used to develop the representations in the model. Each ring in the ellipse was assigned different TMA measured CTE values in the x- and y- directions. The concentric ellipses were then stacked side by side unidirectionally to form each layer. Layers were then stacked accordingly to correctly represent the 0-0 cube and the 0-90 cube. A temperature increase in the entire model is then simulated from room temperature to 90°C. Average strain and CTE in the x- and y-direction of the part was then calculated using a python script.

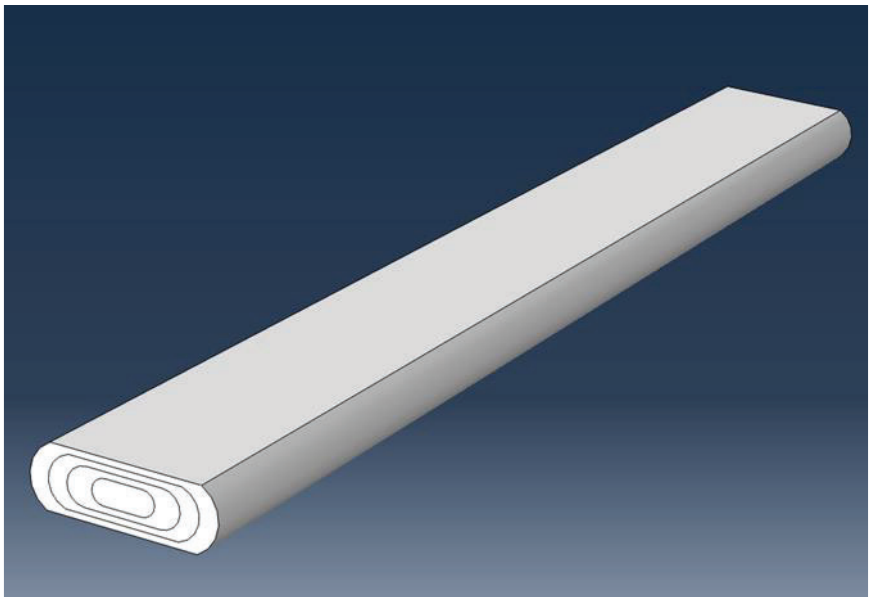

Figure 3 Model used for each bead (made of concentric ellipses)

Experimental and Modelling Results

Strain maps for the 0-0 cube at 90°C are shown in Figure 4. The strain map on the left depicts strain in the x-direction. No significant patterns or artifacts can be seen in the x-strain map. However, when viewing the strain map on the right, the y-strain map, the red banding in the strain map denotes a localized band of high strain that correlates directly to the location of bead-to-bead interfaces. The increased y-strain at the interfaces agrees with literature on LAEDAM, which states the outer surface of a bead has high alignment in the x-direction (22). High alignment in the x-direction means less fibers restricting strain in the y-direction. The average CTE in 0-0 cube was calculated to be 14.4 µm/m°C in the x-direction and 57.7 µm/m°C in the y-direction.

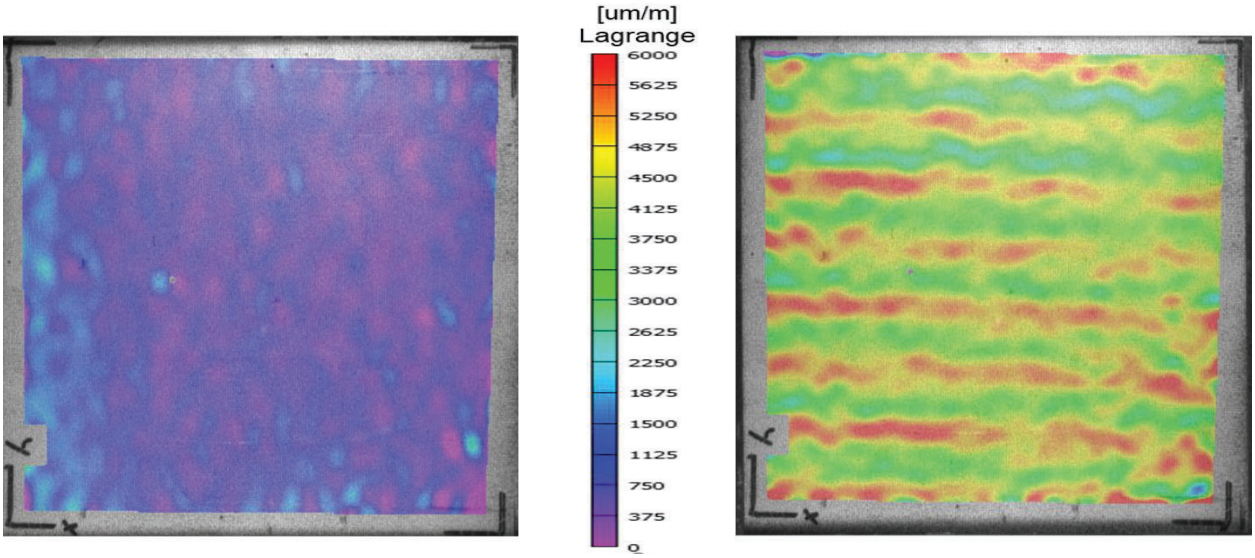

Figure 4 Strain maps of the 0-0 cube at 90 °C (a) x-direction, (b) y-direction

In Figure 5 strain maps for the 0-90 cube at 90°C are shown. Strain in the x-direction of the 0-90 cube, like the x-strain in the 0-0 cube, shows no distinct patterns or artifacts, but has a larger range of strain values. Similarly, bead interfaces can also be seen in the y-strain map of the 0-90 cube, this can be attributed to the beads of the face being imaged. Variation in the y-strain is also greater, likely due to contact with the beads in the adjacent layer restricting movement where contact is occurring. The CTE for the 0-90 cube is 23.7 µm/m°C in the x-direction and 23.8 µm/m°C in the y-direction.

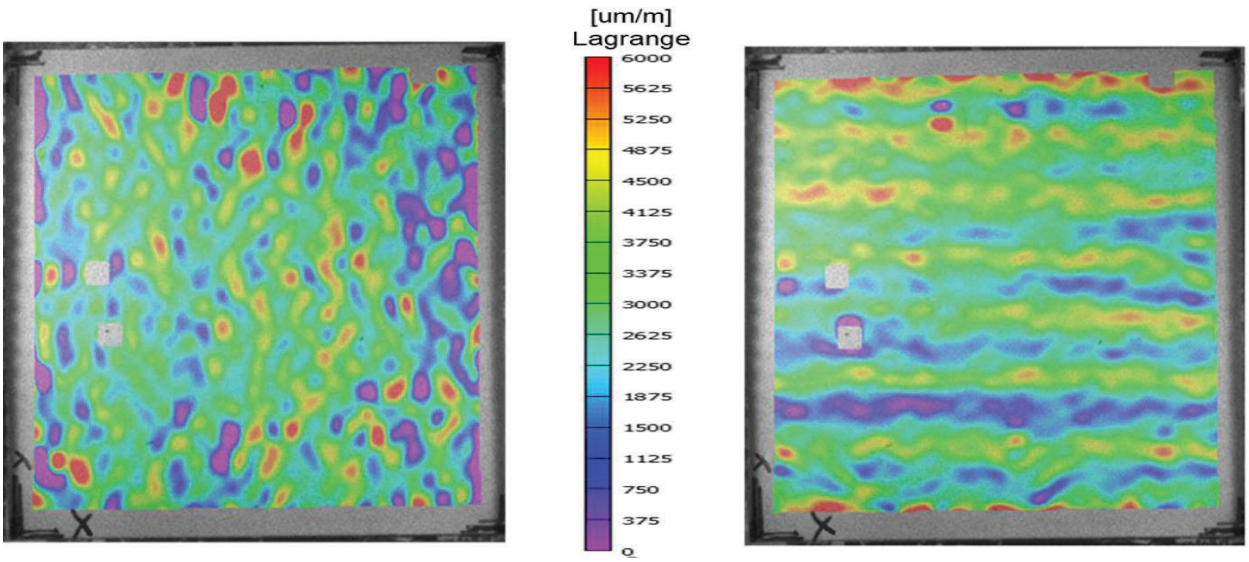

Figure 5 Strain maps of the 0-0 cube at 90 °C (a) x-direction, (b) y-direction

TMA samples in the same position in the width (1,5 & 2,6) of the bead were treated as the same data point for CTE in the x- and y-direction for a total of seven data points across the bead. A graph of the seven data points, including standard error bars, is displayed in Figure 6. The decreased x-direction CTE near the outside of the bead and increased y-direction CTE

agrees with increased fiber alignment in the print direction near the exterior of the bead. The center of the bead exhibits much more comparable x- and y-CTEs. Neither x- nor y-CTEs were symmetric about the center of the bead, which is important in future modelling work.

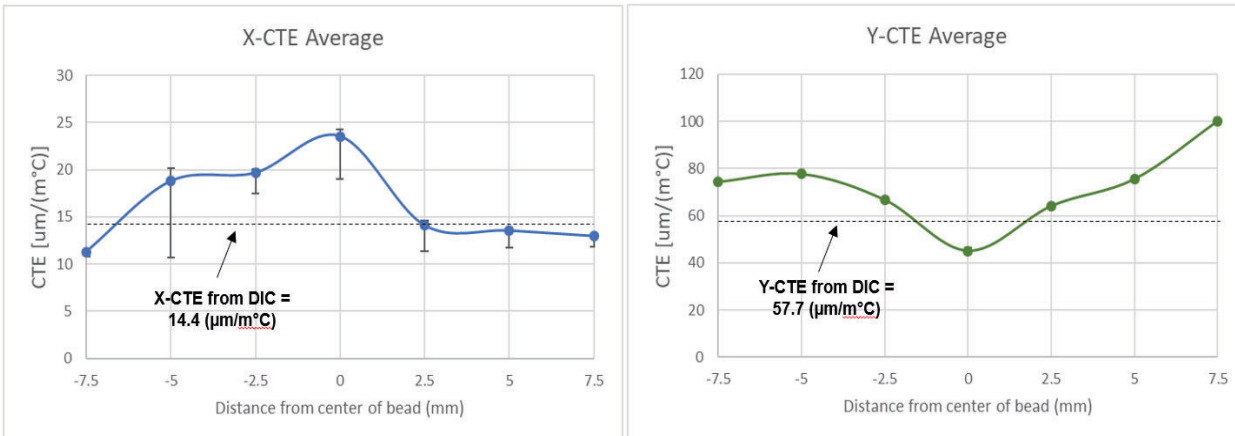

Figure 6 Graphs of x and y CTEs as a function of position within the bead with standard error bars

For the concentric ellipses, each shell's CTE values were calculated by averaging the samples that are the same distance from the center of the bead (i.e. -2.5 and 2.5). X- and y-strain maps for the 0-0 and 0-90 FEA models look very similar to the DIC measure strain maps, which shows promise for this modeling technique. 0-0 y-strain map can be seen in Figure 7. The calculated x-CTE value for the FEA model of the 0-0 cube is very similar to the DIC measured x-CTE. However, the y-CTE value in the 0-0 and the x- and y-CTE values are not very similar, most likely due inter-bead porosity not being accounted for in the FEA model. The DIC and FEA CTE values presented in Table 1.

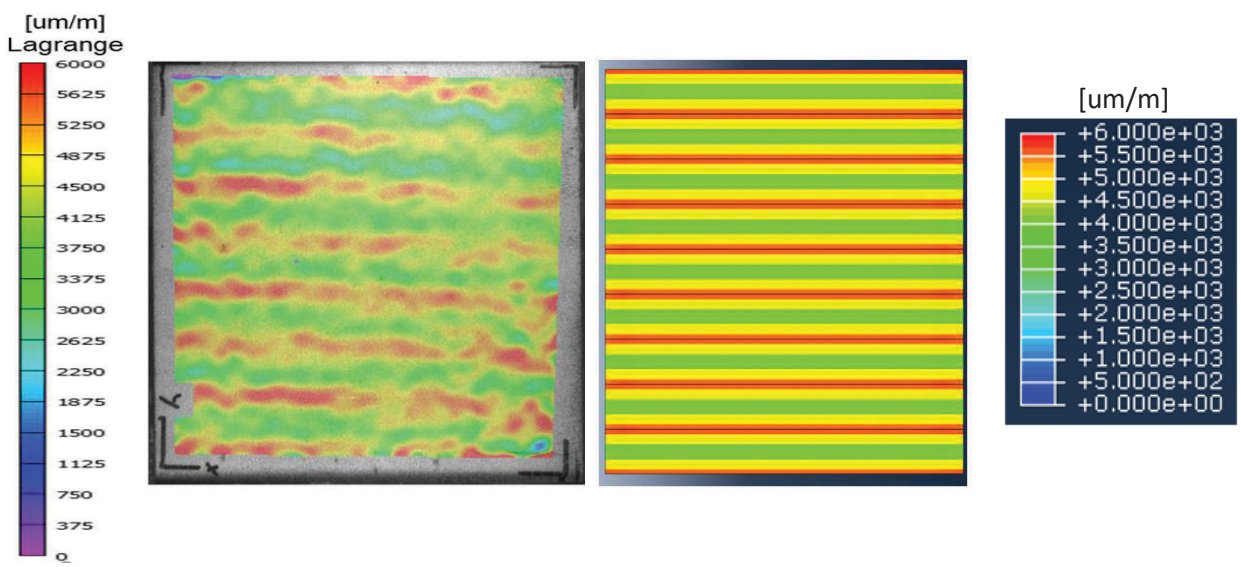

Figure 7 Comparison of FEA and DIC strain maps

Table 1 FEA calculated and DIC measured CTE values

	0-0 Cube		0-90 Cube	
	X-CTE (µm/m°C)	Y-CTE (µm/m°C)	X-CTE (µm/m°C)	Y-CTE (µm/m°C)
DIC	14.4	57.7	23.7	23.8
FEA	15.7	74.1	45.0	45.0

Conclusion

The ability to predict the thermal expansion of a LAEDAM printed part is essential to utilizing the process to create parts where the range of temperatures will be experienced, and geometrical tolerances are of concern. This work has laid a foundation for the use of concentric ellipses to model the variation of properties throughout a printed bead and using these beads as the building blocks for the part exactly as in the actual printing process. It is also apparent from the data presented that CTE can change by up to 100% depending on the sample location within the bead and fiber orientation may not be symmetric in a LAEDAM bead. Although the CTE results of the FEA and the DIC are not extremely similar, likely due to the fact that porosity in the measured cubes was not accounted for in the FEA model. Taking into account the porosity factor in the FEA model will be the goal of future work to create a more accurate model.

Research sponsored by the U.S. Department of Energy, Office of Energy Efficiency and Renewable Energy, Industrial Technologies Program, under contract DE-AC05-00OR22725 with UT-Battelle, LLC. Material provided by Techmer PM, a materials design and manufacture company headquartered in Clinton, TN. Printed on a Cincinnati BAAM printer.

References

1. Popescu, D., et al., FDM process parameters influence over the mechanical properties of polymer specimens: A review. Polymer Testing, 2018. 69: p. 157-166.DOI:https://doi.org/10.1016/j.polymertesting.2018.05.020

2. Ahn, S.-H., et al., Anisotropic material properties of fused deposition modeling ABS. Rapid prototyping journal, 2002. 8(4): p. 248-257

3. Torrado, A.R. and D.A. Roberson, Failure Analysis and Anisotropy Evaluation of 3D-Printed Tensile Test Specimens of Different Geometries and Print Raster Patterns. Journal of Failure Analysis and Prevention, 2016. 16(1): p. 154-164.DOI:10.1007/s11668-016-0067-4

4. Huang, B. and S. Singamneni, Raster angle mechanics in fused deposition modelling. Journal of Composite Materials, 2015. 49(3): p. 363-383.DOI:10.1177/0021998313519153

5. Rezayat, H., et al., Structure-mechanical property relationship in fused deposition modelling. Materials Science and Technology, 2015. 31(8): p. 895-903.DOI:10.1179/1743284715y.0000000010

6. Zaldivar, R.J., et al., Influence of processing and orientation print effects on the mechanical and thermal behavior of 3D-Printed ULTEM® 9085 Material. Additive Manufacturing, 2017. 13: p. 71-80.DOI:10.1016/j.addma.2016.11.007

7. Brenken, B., et al., Fused filament fabrication of fiber-reinforced polymers: A review. Additive Manufacturing, 2018. 21: p. 1-16.DOI:https://doi.org/10.1016/j.addma.2018.01.002

8. Jiang, D. and D.E. Smith, Anisotropic mechanical properties of oriented carbon fiber filled polymer composites produced with fused filament fabrication. Additive Manufacturing, 2017. 18: p. 84-94.DOI:https://doi.org/10.1016/j.addma.2017.08.006

9. Tekinalp, H.L., et al., Highly oriented carbon fiber–polymer composites via additive manufacturing. Composites Science and Technology, 2014. 105: p. 144-150.DOI:10.1016/j.compscitech.2014.10.009

10. Ning, F., et al., Additive manufacturing of carbon fiber reinforced thermoplastic composites using fused deposition modeling. Composites Part B: Engineering, 2015. 80: p. 369-378.DOI:https://doi.org/10.1016/j.compositesb.2015.06.013

11. Duty, C.E., et al., Structure and mechanical behavior of Big Area Additive Manufacturing (BAAM) materials. Rapid Prototyping Journal, 2017. 23(1): p. 181-189.DOI:doi:10.1108/RPJ-12-2015-0183

12. Love, L.J., et al., The importance of carbon fiber to polymer additive manufacturing. Journal of Materials Research, 2014. 29(17): p. 1893-1898.DOI:10.1557/jmr.2014.212

13. A., R., A.-K. A., and G. M., Rheology of fiber suspensions in viscoelastic media: Experiments and model predictions. J. Rheol., 2001. 45: p. 945

14. Ajinjeru, C., et al., The influence of dynamic rheological properties on carbon fiber-reinforced polyetherimide for large-scale extrusion-based additive manufacturing. The International Journal of Advanced Manufacturing Technology, 2018.DOI:10.1007/s00170-018-2510-z

15. Barnes, H.A., A review of the rheology of filled viscoelastic systems. Rheology reviews, 2003: p. 1-36

16. Kim, J.K. and J.H. Song, Rheological properties and fiber orientations of short fiber-reinforced plastics. Journal of Rheology, 1997. 41(5): p. 1061-1085.DOI:10.1122/1.55082517.

Wang, Z. and D. Smith, Rheology effects on predicted fiber orientation and elastic properties in large scale polymer composite additive manufacturing. Journal of Composites Science, 2018. 2(1): p. 10

18. Heller, B.P., D.E. Smith, and D.A. Jack, Effects of extrudate swell and nozzle geometry on fiber orientation in Fused Filament Fabrication nozzle flow. Additive Manufacturing, 2016. 12: p. 252-264.DOI:https://doi.org/10.1016/j.addma.2016.06.005

19. Russell, T., et al., Prediction of the Fiber Orientation State and the Resulting Structural and Thermal Properties of Fiber Reinforced Additive Manufactured Composites Fabricated

Using the Big Area Additive Manufacturing Process. Journal of Composites Science, 2018. 2(2): p. 26

20. Mortazavian, S. and A. Fatemi, Effects of fiber orientation and anisotropy on tensile strength and elastic modulus of short fiber reinforced polymer composites. Composites Part B: Engineering, 2015. 72: p. 116-129.DOI:https://doi.org/10.1016/j.compositesb.2014.11.041

21. Hill, R., Elastic properties of reinforced solids: Some theoretical principles. Journal of the Mechanics and Physics of Solids, 1963. 11(5): p. 357-372.DOI:https://doi.org/10.1016/0022-5096(63)90036-X

22. Tekinalp, H.L., et al., Highly oriented carbon fiber–polymer composites via additive manufacturing. Composites Science and Technology, 2014. 105: p. 144-150.DOI:10.1016/j.compscitech.2014.10.009